Catalysis Science & Technology

Accepted Manuscript

ROYAL SOCIETY OF CHEMISTRY

www.rsc.org/catalysis

Facile Synthesis of $CuCr_2O_4$ Spinel Nanoparticles: A Recyclable Heterogeneous Catalyst for One Pot Hydroxylation of Benzene

Shankha S. Acharyya,[a] Shilpi Ghosh,[a] Shubhadeep Adak,[a] Takehiko Sasaki[b] and Rajaram Bal[a,*]

[a]Catalytic Conversion & Processes Division, CSIR-Indian Institute of Petroleum, Dehradun 248005, India

[b]Department of Complexity Science and Engineering, Graduate School of Frontier Sciences, The University of Tokyo, Kashiwanoha, Kashiwa-shi, Chiba 277-8561, Japan

[*] Mr. Shankha Shubhra Acharyya, Ms. Shilpi Ghosh, Prof. Dr. Takehiko Sasaki, Dr. Rajaram Bal

Corresponding author. Tel.: +91 135 2525917; Fax: +91 135 2660202

E-mail addresses: raja@iip.res.in

Keywords: $CuCr_2O_4$ spinel • nanoparticles • hydroxylation • benzene • phenol

Abstract: A facile hydrothermal synthesis method is developed to prepare $CuCr_2O_4$ spinel nanoparticles catalyst with size between 25-50 nm. Detailed characterization of the material was carried out by XRD, ICP-AES, XPS, EXAFS, SEM, TEM, and TGA. XRD revealed the formation of $CuCr_2O_4$ spinel phase and TEM showed the particle size of 20-50 nm. The catalyst was highly active for selective oxidation of benzene to phenol with H_2O_2. The influence of reaction parameters such as temperature, solvent, substrate to oxidant molar ratio, reaction time, etc. were investigated in detail. The reusability of the catalyst was tested by conducting same experiments with the spent catalyst and it was found that the catalyst did not show any significant activity loss even after 5 reuses. A benzene conversion of 72.5% with 94% phenol selectivity was achieved over this catalyst at 80 ºC temperature. However, significant H_2O_2 decomposition occurs on the catalyst necessitating its usage in five-fold excess.

Introduction

Materials exhibit fascinating properties at the nanoscale differs entirely from their bulk counterparts, owing to quantum size and surface effect.[1] Controlled synthesis of inorganic nanoparticles (NP), is an important goal of modern material chemistry due to their size and shape dependent physical properties and diverse applications. The simple preparation method is required for easy manipulation of the nucleation and growth kinetics for tunable shape and

size of the nanoparticles.[2] Bimetallic NPs, emerging as a new class of materials and show much potential interest compared to the monometallic ones as they exhibit new properties due to synergy between the two metals.[3] Compared to the monometallic NPs, synthesis of high-quality bimetallic ones with controllable size, morphology, composition and structure is much more complicated; therefore, a simple, reliable preparation is still remains a challenge for the researchers.[4] Copper chromium mixed oxides with a spinel structure had been recognized as an important class of bi-metallic oxides that act as a versatile catalyst.[5] Apart from its usage in chemical industries, copper chromite is extensively used as a burn rate modifier in solid propellant processing for space launch vehicles globally.[6] The higher activity of copper chromite is attributed to the tetragonally distorted normal spinel structure [6b,7] with c/a < 1(where a and c are lattice constants in a unit cell along x and z axes respectively) and the arrangement of copper in its structure.[8] A variety of synthetic methods have been employed in the preparation of Cu-Cr catalysts, such as Adkins' method, template method, sol-gel method, co-precipitation method etc.[6,9] Among these methods, the sol–gel method has promising potential for the synthesis of mixed oxides,[10] as relatively low calcination temperature required and the final product also shows high purity and good chemical homogeneity. Previously, the sol–gel method has employed using metal alkoxide precursors that readily undergo catalyzed hydrolysis and condensation to form a sol of metal oxide nanoparticles. But, preparation of Cu-Cr nanoparticles using alkoxide precursors has been limited because many of the metal alkoxides are expensive and sensitive to moisture, heat, and light and making it difficult for long-term storage and for other applications. In addition, some metal alkoxides are not commercially available or are difficult to prepare.[9c] The hydrothermal route is one of the most efficient methods to obtain well-defined nanoparticles with controlled morphologies[11] and recently, we have reported the preparation

of copper nanoclusters supported on nanocrystalline chromium oxide in hydrothermal synthesis method.[12]

Herein we report the preparation of $CuCr_2O_4$ spinel nanoparticles by hydrothermal synthesis method. This preparation method is simple, reproducible and produces high yield (98%) and can be prepared in a large scale (upto 20 g). Furthermore, the catalyst prepared in this process is devoid of leaching properties due to its extremely stable spinel phase. To the best of our knowledge, there is no report for the preparation of $CuCr_2O_4$ spinel nanoparticles with size between 20-50 nm using surfactant promoted hydrothermal synthesis method.

Selective oxidation of inactive hydrocarbons to industrially important intermediates still remains a major challenge.[13] Among these oxygenates, phenol is the most desirable and value-added product due to its widespread use in the fields of resin, plastics, pharmaceuticals, agrochemicals, etc.[14] Industrially, phenol is produced by cumene process. The cumene process is performed by first the reaction of benzene with propene on acid catalysts such as MCM-22, second auto-oxidation of the obtained cumene to form explosive cumene hydroperoxide, and finally the decomposition of cumene hydroperoxide to phenol and acetone in sulfuric acid.[15] Apart from multistep nature, this process suffers from low yield (~5% based on the amount of benzene initially used) and produces explosive intermediate, cumene hydroperoxide and by-products. So, the one-step process for the direct conversion of benzene to phenol is an area of great potential interest and therefore, regarded as one of the ten most challenges of catalysis.[13e] Although there have been several reports using different oxidizing agents like N_2O,[16] H_2O_2,[17] NH_3+ O_2,[18] air+CO [19] etc. but most of the cases phenol yield is very low because phenol is more reactive towards oxidation than benzene, over oxidation products are usually formed,[20] and rapid deactivation of the catalyst by coke deposition during gas phase reaction occurs.[21] The use of H_2O_2 as oxidizing agent in liquid

phase hydroxylation of benzene is of great advantage from both environmental and industrial viewpoint.[22] Bianchi et al. have developed a water-acetonitrile biphasic reaction method in which $FeSO_4$, soluble in the aqueous medium, was used as catalyst and H_2O_2 as oxidant.[23] By employing this method, a significant selectivity to phenol (97%) was observed, although the benzene conversion was 8.6%. Zhang et al. reported a benzene conversion of 34.5 % with a selectivity of 100% towards the phenol using H_2O_2 as oxidant in a mixture of glacial acetic acid and acetonitrile, over Keggin-type molybdovanadophosphoric heteropoly acids.[24] Recently, Borah et. al reported a benzene conversion of 27% and a phenol selectivity of 100% over vanadyl-complex grafted on periodic mesoporous organosilica.[25] Our previous report indicated that copper nanoclusters supported on nanocrystalline chromium oxide catalyst is very efficient in activating C_{sp3}-H bond in the presence of H_2O_2.[12] But this catalyst underwent severe leaching, when it was employed in benzene hydroxylation reaction. Apart from high yield of phenol, recyclability of the catalysts, product separation and maintaining efficiency of H_2O_2 are major issues in liquid phase benzene hydroxylation; therefore, production of phenol by direct hydroxylation of benzene in liquid phase with both high activity and selectivity using heterogeneous catalyst(s) is a major challenge.

We also report the direct hydroxylation of benzene to phenol using the so prepared $CuCr_2O_4$ spinel nanoparticles catalyst with H_2O_2 as oxidant to get a benzene conversion of 72.5% and phenol selectivity of 94%, with a phenol yield of 68%.

Experimental

Materials

Hydrogen Peroxide (50 wt % in water) was purchased from Merck KGaA, Darmstadt, Germany. $Cu(NO_3)_2 \cdot 5H_2O$, $Cr(NO_3)_3 \cdot 9H_2O$, cetyltrimethylammonium bromide, hydrazine,

ammonium hydroxide, benzene (purity > 99.9%), acetonitrile (HPLC grade) were purchased from Sigma-Aldrich Co. All the chemicals were used without further purification.

Catalyst preparation

The $CuCr_2O_4$ spinel nanoparticles were prepared hydrothermally by modifying our own preparation method taking nitrate precursors of copper and chromium.[12] All chemicals were used without further purification. All solvents used were of reagent grade. All syntheses were carried out under ambient conditions. In a typical synthesis procedure, an aqueous solution of 1.5 g $Cu(NO_3)_2.3H_2O$ (from Sigma Aldrich) was added with vigorous stirring to 5.0 g $Cr(NO_3)_3.9H_2O$ (from Sigma Aldrich) dissolved in 26 g deionized water to give a clear dark blue homogeneous solution. By gradual addition of few drop ammonia solution, the pH of the solution was made 8. An ethanolic solution (10%) of 1.7 g CTAB (from Sigma Aldrich) was added dropwise followed by addition of 0.4 g hydrazine (from Sigma Aldrich) to the reaction mixture. The reagents were added maintaining the molar ratio of Cu: Cr: CTAB: H_2O: hydrazine = 1: 2: 0.75: 250: 1. After stirring, the so obtained homogeneous solution was hydrothermally treated at 180 °C for 24 h in a Teflon-lined autoclave vessel under autogeneous pressure. The solid product was collected by means of centrifugation at 18,000 rpm and dried at 120 °C, for 10 h, followed by calcination at 750 °C for 6 h in air (ramped at 1° C/min) to get $CuCr_2O_4$ spinel nanoparticles.

Characterization techniques

Powder X-ray diffraction spectra were collected on a Bruker D8 advance X-ray diffractometer fitted with a Lynx eye high-speed strip detector and a Cu K_α radiation source with a wavelength of 1.5418 Å. Diffraction patterns in the 2°–80°region were recorded at a rate of 0.5 degrees (2q) per minute. The resulting XRD profiles were analyzed to identify the crystal phase of the compound using reference standards. The line width of the most intense

XRD peak was taken for estimation of crystallite size by the Scherrer equation.Scanning electron microscopy (SEM) images were taken on a FEI Quanta 200 F, using tungsten filament doped with lanthanumhexaboride (LaB_6) as an X-ray source, fitted with an ETD detector with high vacuum mode using secondary electrons and an acceleration tension of 10 or 30 kV. Samples were analyzed by spreading them on a carbon tape. Energy dispersive X-ray spectroscopy (EDX) was used in connection with SEM for the elemental analysis. The elemental mapping was also collected with the same spectrophotometer.Transmission electron microscopy (TEM) images were collected using a JEOL JEM 2100 microscope, and samples were prepared by mounting an ethanol-dispersed sample on a lacey carbon Formvar coated Cu grid. The particle size and distribution of the samples were analyzed by TEM.

X-ray photoelectron spectroscopy (XPS) spectra were recorded on a Thermo Scientific K-Alpha X-Ray photoelectron spectrometer. The resulting spectra were analyzed to identify the different oxidation states of the copper and chromium ions present in the sample. Prior to the analysis, the spectra were calibrated with reference to C1s observed at a binding energy of 284.5 eV. The uncertainty on the energy values was $\pm$ 0.15 eV. Extended X-ray absorption fine structure spectroscopy (EXAFS) measurements of Cu-K edge were carried out at the High Energy Accelerator Research Organization (KEK-IMMS-PF). The measurement was made at transition mode and spectra were taken at BL-7C and BL-9C. The electron storage ring was operated at 2.5 GeV and 450 mA, synchrotron radiation from the storage ring was monochromatized by a Si (111) channel cut crystal. Ionized chamber, which were used as detectors for incident X-ray (I_o) and transmitted X-ray (I), were filled with N_2 mixture gas, respectively. The angle of the monochromators was calibrated with Cu foil. The EXAFS raw data were analyzed with UWXAFS analysis package including background subtraction program AUTOBK and curve fitting program FEFFIT.[26] The amplitude reducing factor, S_o^2 was fixed at 1.0. The backscattering amplitude and phase shift were calculated theoretically

by FEFF 8.4 code.[27] ATOMS were used to obtain FEFF input code for crystalline materials.[28] Chemical analyses of the metallic constituents were carried out by Inductively Coupled Plasma Atomic Emission Spectrometer (ICP-AES); model: PS 3000 uv, (DRE), Leeman Labs, Inc, (USA). Thermo gravimetric analyses (TGA) of the uncalcined catalyst were carried out in a Pyris Diamond, Perkin Elmer Instruments, and Technology by SII (Seiko Instruments Inc), USA instrument-balance by heating 2.15 mg samples at 5 °C min^{-1} in flowing air. Fourier transform infra-red (FT-IR) spectra were recorded on a Thermo Nicolet 8700 (USA) instrument with the operating conditions: resolution: 4 cm^{-1}, scan: 36, operating temperature: 23–25 °C and the frequency range: 4000-400 cm^{-1}. Spectra in the lattice vibrations range were recorded for wafers of sample mixed with KBr. ^1H and 13C NMR spectra were recorded on a Bruker Avance 500 Spectrometer in $CDCl_3$ with $CHCl_3$ (7.27 ppm for ^1H) as a standard and the chemical shifts are expressed in δ parts per million relative to tetramethylsilane (TMS) as the internal standard. All yields refer to the isolated products.

Liquid phase hydroxylation

Liquid phase oxidation reaction was carried out in a two neck round bottom flask, equipped with refrigerant, containing 0.1 g catalyst, 10 ml solvent and 1 g benzene to which H_2O_2 (50% aq. solution) was added dropwise to prevent immediate H_2O_2 decomposition. The flask was then emerged in a preheated oil bath and vigorously stirred with a magnetic stirrer. The reaction temperature was ranged between RT and 100 °C. Small aliquots of the sample were withdrawn from the reaction mixture at regular intervals for analysis using a syringe. At the end of the reaction, the solid particles (catalyst) were separated by filtration and the products were analysed by Gas Chromatograph (GC, Agilent 7890) connected with a HP5 capillary column (30m length, 0.28 mm id, 0.25 µm film thickness) and flame ionisation detector (FID). Chem Station software was used to collect and analyze the respective GC-data. The

relative error of product determination did not exceed ±5%. The benzene conversion and phenol formation were calculated using a calibration curve (obtained by manual injecting the authentic standard compounds). An anisole solution with a known amount was used as an external standard for analysis. The individual yields were calculated and normalized with respect to the GC response factors. The product identification was carried out by injecting the authentic standard samples in GC and GC-MS. The product was separated from the reaction mixture by means of column chromatography and was further confirmed by ^{1}H NMR. For the reusability test, the catalyst was repeatedly washed with acetonitrile and acetone and dried overnight at 110 °C and used as such, without regeneration. In order to check the metal leaching the mother liqor was then analyzed using ICP-AES.

Material Balance

We have performed the C-balance for the most of the experiments and have also done the material balance for few experiments. The estimated error in analysis arising due to sampling and handling losses was $\pm$ 5%.

Results and discussion

Generation of $CuCr_2O_4$ Spinel Nanoparticles

The $CuCr_2O_4$ spinel nanoparticles catalyst was prepared using nitrate precursors of copper and chromium in aqueous medium, varying our own preparation method.[12] It is believed that, the precursors of copper and chromium ionizes and counter ions diffuse into the aqueous solution, maintaining the homogeneity of the medium. When concentration of the micelles was less than that of critical micelle concentration (CMC), Cu^{2+} and Cr^{3+} ions are preferentially located at the micellar surface due to presence of Br^{-} ions.[29] The growth of the

particles occurs along the side of the particles, which is exposed to water. When concentration of the surfactant becomes ≥ CMC, the aqueous medium is largely populated by surfactant micelles. The Cu and Cr-precursor ions approach towards the micellar headgroup region. In this situation, growth in a particular direction is prohibited due to the micellar steric effects and the nanoparticles are allowed to grow to form spherical nanoparticles with limited size. Basic medium influences the role of CTAB [30] and hydrazine forms complexes with Cu^{2+} ions [31] and thereby prohibits Ostwald ripening process to a certain extent (Scheme S1, Supporting Information).[32] However, change in the concentration of any one of the gel components (Cu, Cr, CTAB, hydrazine), leads to the formation of the mixed metal oxides without forming the pure spinel phase;[12] and their respective morphologies can be distinguished from their SEM images (Figure S4, Supporting Information).

Catalyst Characterization

The physicochemical properties of the $CuCr_2O_4$ material is shown in Table 1. The crystalline phase, degree of crystallinity and phase purity were determined by X-ray diffraction (XRD). The X-ray diffraction patterns of the Cu-Cr catalysts are presented in Figure 1. XRD pattern showed the typical diffraction lines of the bulk, single phased $CuCr_2O_4$ spinel (Figure 1)(JCPDS. 05-0657). No impurity phase such as $CuCrO_2$ and not even cubic or monoclinic $CuCr_2O_4$ was found.The particle size was determined from the full width half maxima of the line broadening corresponding to the diffraction angle of 46.62° by using Scherrer equation and a mean particle size (crystallite size) of 38 nm was observed. XRD diffractogram (Figure 1b) also predicts that, the catalyst retains its spinel phase even after 5 recycles, which was furthermore supported by EXAFS analysis (Table 2 & Figure S7, Supporting Information).

The $CuCr_2O_4$ spinel nanoparticles catalyst, prepared hydrothermally in the presence of cetyltrimethylammonium bromide (CTAB) surfactant showed a single-phase morphology

reflecting an assembly effect of the surfactant as imaged by SEM (Figure 2 & Figure S1-S3, Supporting Information). SEM images of the catalyst (Figure 2) showed the formation of almost homogeneously distributed uniform particles with size ~35 nm. From EDAX image (Figure S4, Supporting Information), it can be seen that the sample contains only Cu, Cr and O and the elemental mapping demonstrated the homogeneous distribution of Cu and Cr in the catalyst (Figure S5, Supporting Information). The SEM images also confirmed that the $CuCr_2O_4$ spinel nanoparticles are entirely different from the inhomogeneous disordered morphology of commercial and conventional catalysts (Figure S1, Supporting Information). Notably, the SEM images also revealed the fact that NH_4OH, CTAB, hydrazine have direct role in directing the particle size and overall topology of the catalyst (as evident from Figure S2, Supporting Information). SEM images of Cu-Cr samples prepared by non-hydrothermal process (Figure S3, Supporting Information) show that the particles are non uniform; so we believe that the autogeneous pressure during hydrothermal condition is necessary for the generation of uniformity of the $CuCr_2O_4$ spinel nanoparticles.

The representative Transmission Electron Microscopy (TEM) of the catalyst is shown in Figure 3. The TEM image showed that the catalyst was comprised of almost uniform type of particles with average size of 35 nm. The particle size distributions histogram is shown in Figure 4. The lattice fringe with a d-spacing of 0.30 nm corresponding to [220] plane of $CuCr_2O_4$ spinel with diffraction angle (2θ) of 29.6 is also presented (Figure 3c).[6a] Moreover, the TEM image of the spent catalyst (after 5 recycle) (Figure 3d) revealed that the particle size of the $CuCr_2O_4$ spinel was almost unchanged during the catalysis (Table 1).

The catalyst surface composition and oxidation state were investigated by XPS. The XPS binding energies (BE) with characteristic core levels of Cu, Cr and O (Figure 5 & 6 and Figure S6, Supporting Information respectively) in the $CuCr_2O_4$ sample is presented. The

Cu2p spectrum of the fresh sample is characterized by two spin orbit doublets with strong satellite peaks. The so obtained $Cu2p_{3/2}$ signals fitted satisfactorily to two principal peak components at ~ 935.3 and 933.8 eV. The BE for the Cu2p peak is in close agreement with that of $CuCr_2O_4$ indicating that, the main phase is $CuCr_2O_4$ spinel. The low energy component with $Cu2p_{3/2}$ at 933.8 eV is associated to Cu^{2+} in octahedral sites, whereas the high component at 935.3 eV is associated to Cu^{2+} in tetrahedral sites.[33] The $Cr2p_{3/2}$ signal (BE at 576.6 eV) clearly indicated the presence of Cr^{III} in the catalyst. The O1s signal of the catalyst showed two almost overlapping peaks at 532.2 and 530.2 eV, assigned to lattice oxygen ions in different chemical environments. These results are in accord with the formation of a mixed copper chromium oxide, $CuCr_2O_4$,[33,34] and also supported the XRD analysis.

Cu K-edge extended X-ray absorption fine structure (EXAFS) spectroscopic analysis of the catalyst supports the formation of $CuCr_2O_4$ spinel and the spinel structure remains unchanged during the catalysis. Detailed structural parameters of the curve fitting results are summarized in Table 2 and Figure S7, Supporting Information. The EXAFS spectrum analyzed as the superposition of the crystal phase of $CuCr_2O_4$ and the dual CuO phase. The small coordination number 2.5 for the CuO phase indicates that the CuO phase corresponds to the surface layer of oxidized Cu on $CuCr_2O_4$ crystal or the monatomically dispersed CuO on the $CuCr_2O_4$ crystal phase. From Cu2p XPS spectra, tetrahedrally coordinated Cu and the octahedrally coordinated Cu are assigned to the $CuCr_2O_4$ phase and the surface CuO phase, respectively. The coordination number for CuO was found to be smaller than the value 4-6 in the present study, because it is minor phase as compared to the $CuCr_2O_4$.

The association of the CTAB molecules on the uncalcined catalyst can be analyzed by the FTIR analysis (Figure 7). A comparison of the FTIR- spectra of dried uncalcined sample, with that of pure CTAB was analyzed, which not only confirmed the presence, but also

revealed the nature of interaction of CTA- molecules with the Cu-Cr surface. The peaks of the sample at 809, 1062 cm^{-1} can be assigned to the C-N^+ stretching modes of CTA- molecules.[35] The peak at 1378 and at 1462 cm^{-1} were assigned to symmetric mode of vibration of the head groups of the methylene moiety (N^+—CH_3) and CH_2 scissoring mode respectively.[35] The frequencies above 1600 cm^{-1} to 3000 cm^{-1} can be attributed due to CH_2 symmetric antisymmetric vibrations region. It is to be noted that, the shift of vibrations to lower frequency suggested that, alkyl chains experienced a more hydrophobic environment in Cu-Cr blocks upon the surface of which the CTA- moieties were supposed to be bounded.[35] These typical frequencies were absent when the material was calcined at 750 °C in air (fresh catalyst) in the case of the prepared catalyst, which indicated that, the embedded CTAB moieties have been completely removed from the catalyst surface during calcination. The calcined sample also exhibited absorption bands at 608 and 517 cm^{-1}, which refer to the $Cr_2O_4^{2-}$ group in spinel.[6a] Moreover, it was also confirmed from the FTIR diagram that, there was no structural deformation in the catalyst even after 5 recycles. Furthermore, in the SEM-EDAX diagram of the fresh catalyst (Figure S4, Supporting Information) does not show any peak for C, N or even Br, which further confirms the removal of the template (CTAB) by calcination. The embedment of CTAB molecules on the pre-calcined catalyst surface was further confirmed from TGA analysis. TGA analysis was operated to understand the decomposition behavior of the sample in Figure S8, Supporting Information. The TGA diagram showed that the weight loss occurs in three stages, first being the loss of water followed by the decomposition of reactants to form NO_x and organic phases at 150 to 250 °C and finally the combustion of CTA- between 250°–350 °C. A further small mass loss is noticed between 400°–550 °C due to the elimination of remaining carbon and organic compounds. No weight loss was observed when the temperature was further increased from

550° to 1000° C, indicating the stability of the catalyst (spinel phase) upto 1000° C. Total mass reduction of 42.7% confirmed the complete the removal of the template CTAB.

Catalytic Activity

The catalytic activities of $CuCr_2O_4$ spinel nanoparticles (Cu-Cr^{NP}) catalyst in the direct hydroxylation of benzene to phenol in liquid phase by using H_2O_2 as oxidant have been summarized in Table 3. At room temperature (35 °C), only 3.5 % of benzene conversion was noticed. With increasing reaction temperature, the yield of the desired product (i.e. phenol) increased. The yield of phenol reached to ~15% at 50 °C and 68% at 80 °C over this catalyst (Figure S9, Supporting Information). Further raising the temperature to 100 °C, there was no marked increase in the conversion of benzene, presumably because of rapid decomposition of H_2O_2 at this temperature; but the selectivity to phenol (Φ_{OH}) decreased sharply to 65.5%, due to the formation of over-oxidized products, namely catachol (cat) and hydroquinone (HQ). The effect of benzene to H_2O_2 molar ratio was studied at 80 °C and it was observed that, more the H_2O_2 concentration, greater the benzene conversion and lesser the selectivity of phenol (Figure S9, Supporting Information). Weight of the catalyst played an important role in benzene hydroxylation reaction. Blank experiment was performed in absence of catalyst; conversion of benzene was too poor to be detected by GC analysis (Table 3, entry 10). Increment of the catalyst weight increased the conversion of benzene; at the same time, selectivity to phenol also decreased (Figure S11, Supporting Information). Maintaining all the optimum conditions, when the reaction was allowed to run for several hours (Figure S12, Supporting Information), we noticed that, although the conversion of benzene increased with time, but phenol selectivity gradually went decreasing. The decrease in phenol selectivity was

not prominent till 10h; after 10h, the phenol selectivity decreased rapidly due to the formation of over-oxidised products of phenol like catechol and hydroquinone.

It is worth mentioning that, small amount of biphenyl was also detected in the reaction mixture when excess amount of H_2O_2 was used. This phenomenon indicates the probable involvement of free-radical mechanism. The hypothesis was confirmed, when we used 2,6-di-*tert*-butyl-4-methyl phenol as a radical scavenger with benzene (10 wt% wrt benzene) was taken. No phenol was detected till 12h. We also observed that, the catalyst was active only in acetonitrile solvent. We believe that, Cu^{2+} in the catalyst framework interacts with the π-electron cloud of benzene. Cr^{3+} is not involved in the reaction but stabilizes the copper ion(s) against aggregation during the reaction condition.[33] H_2O_2 does not interact with benzene at normal condition. H_2O_2 dissociation is believed to occur homogeneously over the $CuCr_2O_4$ catalyst and follows the mechanism, suggested by Kazarnovsky.[36] Dissociation of H_2O_2 over $CuCr_2O_4$ generates the active species $^{\bullet}OH$ (free hydroxy radical).These hydroxy radicals behave as an electrophile in this reaction[37] and attacks the activated C-H bond which is adjacent to the π-system (phenyl ring) by means of homolytic C–H bond cleavage mechanism; thereby hydroxylated benzene i.e. phenol moiety is produced on the surface of the catalyst. Use of excess H_2O_2 increases the dissociation rate, causing an increase of local pH;[38] consequently, generated excess $^{\bullet}OH$ radicals, which attack concomitantly the phenyl radical to produce biphenyl moiety, and thereby explains the presence of biphenyl in the reaction medium.

Notably, commercial Cr_2O_3, CuO, Cu_2O and $CuCr_2O_4$ catalyst did not show any activity (Table 3, entry 1-4). Conventional catalyst prepared by impregnation method also showed negligible activity (Table 3, entry 5). The reason can be attributed to the small size as well as extreme stable spinel phase of the $CuCr_2O_4$ spinel nanoparticles containing non-leachable species. The comparatively smaller size of $CuCr_2O_4$ spinel nanoparticles catalyst possess

comparatively high specific surface area which corresponds to higher dispersion of the catalyst that leads to the availability of more exposed surface active sites, where the catalytic reaction takes place. Inevitably, a higher reaction rate was observed in case of the $CuCr_2O_4$ spinel nanoparticles catalyst. The poor catalytic activity of the impregnated catalyst may be attributed to their irregular shape and larger particles size, which limits the accessibility of the catalyst towards the reacting substrates. Although nanoclusters of Cu (II) supported on nanocrystalline Cr_2O_3 meets this criteria, but the catalyst suffers severe leaching and thus its use is limited in benzene hydroxylation reaction. Commercial $CuCr_2O_4$, although bears spinel phase, it also suffers leaching.

The oxidant, H_2O_2 was used in an excess amount (benzene: H_2O_2 = 1:5 molar ratio). In general, H decomposes spontaneously over a catalytic surface. We did H_2O_2 decomposition test with our catalyst (absence of benzene and solvent) and found that greater than 80% of the H_2O_2 decomposed at the reaction temperature. Hence, we used an excess of H_2O_2 so that the active oxygen species needed for the oxidation of benzene could be available during the reaction. Furthermore, we took the reaction mixture and performed permanganometric titrations to detect H_2O_2, but no H_2O_2 was discovered in the reaction mixture, indicating that the unreacted H_2O_2 molecules have been decomposed completely. We have plotted H_2O_2 consumption in terms of its efficiency (Eo) in Table 3.

Recyclability of the Catalyst

The efficiency of a heterogeneous catalyst is evaluated in terms of its recyclability and stability. The reusability of the catalyst $CuCr_2O_4$ was studied without any regeneration. The catalyst was filtered during hot condition and repeatedly washed with acetonitrile and acetone and dried overnight at 100 ºC and used as such. We observed that the catalyst $CuCr_2O_4$ showed negligible change in its activity (conversion and selectivity, Entry 8, Table 3 and

Figure 8). The amount of Cu and Cr present in $CuCr_2O_4$ catalyst after 5 reuse (estimated by ICP-AES, Cu: 21.8 % by weight and Cr: 43.5 % by weight) is almost same as the fresh catalyst (estimated by ICP-AES, Cu: 22.7 % by weight and Cr: 42.9 % by weight) confirming the true heterogeneity of the catalyst. After 5 recycles, negligible amount of leaching of Cu and Cr was detected by ICP-AES (concentration of both metals were <2 ppb.)

Conclusion

In summary, we have developed a surfactant-promoted simple preparation method to prepare 20-50 nm $CuCr_2O_4$ spinel nanoparticles having high thermal stability and good catalytic activity for the single step conversion of benzene to phenol using H_2O_2, exhibiting 72.5% benzene conversion and 94% selectivity towards phenol at 80 °C. The catalyst can be reused several times without any activity loss. The proposed method is also advantageous from the standpoint of low cost, environmental benignity and operational simplicity; furthermore, it can be applicable to large-scale reactions. This environmentally benign, "green" route to phenol production may be a potential alternative to the existing cumene process.

Acknowledgements

SSA thanks CSIR and SG thanks UGC, New Delhi, India, for their respective fellowships. .B. thanks CSIR, New Delhi, for financial support in the form of the 12 FYP Project (CSC- 0125, CSC- 0117). The Director, CSIR-IIP is acknowledged for his help and encouragement. The authors thank Analytical Section Division, IIP for the analytical services.

References

1 (a) A. P. Alivisatos, *Science,* 1996, **271**, 933–937; (b) R. W. J. Scott, O. M. Wilson and R. M. Crooks, *J. Phys. Chem. B,* 2005, **109**, 692–704; (c) J. F. Parker, C. A. Fields-Zinna and R. W. Murray, *Acc. Chem. Res.,* 2010, **43**, 1289–1296.

2 (a) J. Zhuang, A. D. Shaller, J. Lynch, H. Wu, O. Chen, A. D. Q. Li and Y. C. Cao, *J. Am. Chem. Soc.,* 2009, **131**, 6084–6085; (b) N. Shang, P. Papakonstantinou, P. Wang, A. Zakharov, U. Palnitkar, I. N. Lin, M. Chu and A. Stamboulis, *ACS Nano,* 2009, **3**, 1032–1038.

3 (a) M. Jaime, R. Movshovich, G. R. Stewart, W. P. Beyermann, M. G. Berisso, M. F. Hundley, P. C. Canfield and J. L. Sarrao, *Nature,* 2000, **405**, 160–163; (b) D. Wang and Y. Li, *Adv. Mater.,* 2011, **23**, 1044–1060; (c) D. Xu, Z. P. Liu, H. Z. Yang, Q. S. Liu, J. Zhang, J. Y. Fang, S. Z. Zou and K. Sun, *Angew. Chem.,* 2009, **48**, 4217–4221; (d) B. D. Adams, G. Wu, S. Nigro and A. Chen, *J. Am. Chem. Soc.,* 2009, **131**, 6930–6931.

4 (a) D. S. Wang, Q. Peng and Y. D. Li, *Nano Res.,* 2010, **3**, 574–580; (b) R. Hao, R. Xing, Z. Xu, Y. Hou, S. Gao and S. Sun, *Adv. Mater.,* 2010, **22**, 2729–2742.

5 (a) Y. Liang, H. Wang, J. Zhou, Y. Li, J. Wang, T. Regier and H. Dai, *J. Am. Chem. Soc.,* 2012, **134**, 3517–3523; (b) R. Prasad and P. Singh, *Catal. Rev. Sci.& Eng.,* 2012, **54**, 224–279; (c) E. Santacesaria, G. Carotenuto, R. Tesser and M. Di Serio, *Chem. Eng. J.,* 2012, **179**, 209–220; (d) D. Liu, D. Zemlyanov, T. Wu; R. J. Lobo-Lapidus, J. A. Dumesic, J. T. Miller and C. L. Marshall, *J. Catal*., 2013, **299**, 336–345; (e) Z. Xiao, S. Jin, M. Pang and C. Liang, *Green Chem.,* 2013, **15**, 891–895.

6 (a) A. M. Kawamoto, L. C. Pardini and L. C. Rezende, *Aerosp. Sci. Technol.,* 2004, **8**, 591–598; (b) P.S. Sathiskumar, C. R. Thomas and G. Madras, *Ind. Eng. Chem. Res.,* 2012, **51**, 10108–10116.

7 J. Stroupe, *J. Am. Chem. Soc.,* 1949, **71**, 569–572.

8 A. V. Boldyre, *Combust. Explosive Shock Waves,* 1975, **11**, 611–613.

9 (a) R. Connor, K. Folkers and H. Adkins, *J. Am. Chem. Soc.,* 1932, **54**, 1138–1145; (b) S. Roy and J. Ghose, *Mater. Res. Bull.,* 1999, **34**, 1179–1186; (c) Z. Ma, Z. Xiao, J. A. van Bokhoven and C. Liang, *J. Mat. Chem.,* 2010, **20***,* 755–760.

10 L. Castro, P. Reyes and C. M. de Correa, *J. Sol-Gel Sci. Tech.,* 2002, **25***,* 159–168.

11 X. W. Xie and W. J. Shen, *Nanoscale,* 2009, **1**, 50–60.

12 B. Sarkar, P. Prajapati, R. Tiwari, R. Tiwari, S. Ghosh, S. S. Acharyya, C. Pendem, R. K. Singha, L. N. S. Konathala, J. Kumar, T. Sasaki and R. Bal, *Green Chem.,* 2012, **14**, 2600–2606.

13 (a) R. A. Sheldon and H. van Bekkum, Fine Chemicals through Heterogeneous Catalysis, Wiley-VCH, Weinheim, 2001, pp 1–10; (b) J. M. Thomas, R. Raja, G. Sankar and R. G. Bell, *Nature,* 1999, *398*, 227–230; (c) S. S. Stahl, *Angew. Chem.,* 2004, **43**, 3400–3420; (d) C. Limberg, *Angew. Chem.,* 2003, **42**, 5932–595; (e) E. Roduner, W. Kaim, B. Sarkar, V. B. Urlacher, J. Pleiss, R. Gläser, W. D. Einicke, G. A. Sprenger, U. Beifuß, E. Klemm, C. Liebner, H. Hieronymus, S. F. Hsu, B. Plietker and S. Laschat, *ChemCatChem,* 2013, **5**, 82–112.

14 Ullmann's Encyclopedia of Industrial Chemistry, Wiley-VCH Verlag GmbH & Co. KGaA, Weinheim, 2012, vol. **26**, DOI: 10.1002/14356007.a19_313.

15 M. Tada, R. Bal, T. Sasaki, Y. Uemura, Y. Inada, S. Tanaka, M. Nomura and Y. Iwasawa, *J. Phys. Chem. C,* 2007, **111**, 10095–10104.

16 A. Koekkoek, Q. Yang, R. A. van Santen, C. Li and E. J. M. Hensen, *Chem. Commun*., 2009, 7590–7592.

17 (a) C. Walling, *Acc. Chem. Res*., 1975, **8***,* 125–131; (b) P. T. Tanev, M. Chibwe and T. J. Pinnavaia, *Nature,* 1994, **368**, 321–323; (c) L. Balducci, D. Bianchi, R. Bortolo, R. D'Aloisio, M. Ricci, R. Tassinari and R. Ungarelli, *Angew. Chem.,* 2003, **115**, 5087–5090.

18 (a) R. Bal, M. Tada, T. Sasaki and Y. Iwasawa, *Angew. Chem.,* 2006, **45**, 448–452; (b) L. Wang, T. Sasaki, S. Yamamoto, K. Hayashizaki, S. Malwadkar, M. Tada, S. Nagamatsu and Y. Iwasawa, *ChemCatChem,* 2013, **5***,* 2203–2206.

19 M. Tani, T. Sakamoto, S. Mita, S. Sakaguchi and Y. Ishii, *Angew. Chem.,* 2005*,* **44**, 2586–2588.

20 R. A. Sheldon and J. K. Kochi, Metal-Catalyzed Oxidations of Organic Compounds, Academic Press, New York, 1981, 329–333.

21 G. I. Panov, A. S. Kharitonov and V. I. Sobolev, *Appl. Catal. A,* 1993, **98**, 1–20.

22 (a) J. Piera and J. E. Backvall, *Angew. Chem.,* 2008, **47**, 3506–3523; (b) K. Kamata, K. Yonehara, Y. Nakagawa, K. Uehara and N. Mizuno, *Nature Chem.,* 2010, **2**, 478–483.

23 D. Bianchi, R. Bortolo, R. Tassinari, M. Ricci and R. Vignola, *Angew Chem.,* 2000, **112**, 4491–4493.

24 F. Zhang, M. Guo, H. Ge and J. Wang, *Chin. J. Chem. Eng.* 2007, **15***,* 895–898.

25 P. Borah, X. Ma, K. T. Nguyen and Y. Zhao, *Angew. Chem.,* 2012, **51**, 7756–7761.

26 (a) E. A. Stern, M. Newville, B. Ravel, Y. Yacoby and D. Haskel, *Physica B,* 1995, **117***,* 208–209; (b) M. Newville, P. Livins, Y. Yacoby, E. A. Stern and J. J. Rehr, *Phys. Rev. B,* 1995, **47***,* 14126; (c) A. L. Ankudinov, B. Ravel, J.J. Rehr and S. D. Conradson, *Phys. Rev. B,* 1998, **58***,* 7565.

27 A. L. Ankudinov, A. I. Nesvizhskii and J. J. Rehr, *Phys. Rev. B,* 2003, **67**, 115120.

28 B. Ravel, *J. Synchrotron Rad.,* 2001, **8**, 314–316.

29 S. De and S. Mandal, *Colloids & Surfaces A: Physicochem. Eng. Aspects,* 2013, **421**, 72–83.

30 M. Hashempour, H. Razavizadeh, H. Rezaie, M. Hashempour and M. Ardestani, *Mater. Chem. Phys.,* 2010, **123***,* 83–90.

31 B. T. Heaton, C. Jacob and P. Page, *Coord. Chem. Rev.,* 1996*,* **154**, 193–229.

32 H. Goesmann and C. Feldmann, *Angew. Chem.,* 2010, **49**, 1362–1395.

33 (a) F. Severino, J. Brito, O. Carfas and J. Laine, *J. Catal.,* 1986, **102**, 172–179; (b) F. Severino, J. L. Brito, J. Laine, J. L. G. Fierro and A. J. Lo´pez Agudoy*, J. Catal.,* 1998, **177**, 82–95; (c) G. Pantaleo, L. F. Liotta, A. M. Venezia, G. Deganello, E. M. Ezzo, M. A. El Kherbawi and H. Atia, *Mater. Chem. Phys.,* 2009, **114***,* 604–611.

34 C. C. Chien, W. P. Chuang and T. J. Huang, *Appl. Catal. A: Gen,* 1995, **131**, 73–87.

35 W. Cheng, S. Dong and E. Wang, *Langmuir,* 2003, **12**, 9434–9439.

36 I. A. Kazarnovsky, Dokl. *AN SSSR*. 1975, Vol. **221**, S353 *(in Russian).*

37 A. Dubey, V. Rives and S. Kannan, *J. Mol. Catal. A: Chem.,* 2002, **181**, 151–160.

38 R. Araminaite, R. Garjonyte and A. Malinauskas, *Cent. Eur. J. Chem.,* 2008, **6***,* 175–179.

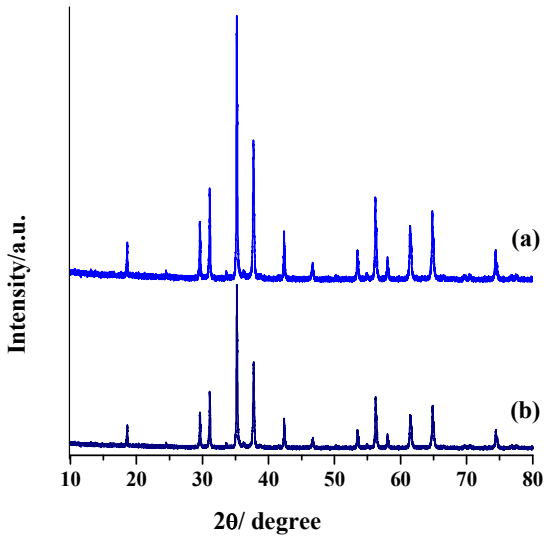

Figure 1. XRD diffractogram of the (a) prepared $CuCr_2O_4$ catalyst and (b) spent catalyst (after 5 recycles).

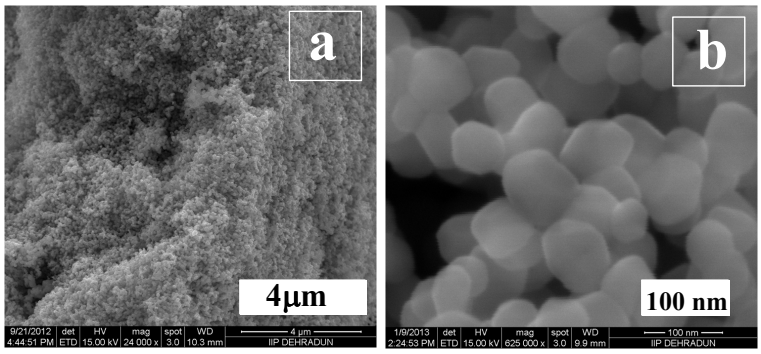

Figure 2. SEM images of the $CuCr_2O_4$ spinel nanoparticles at different magnifications.

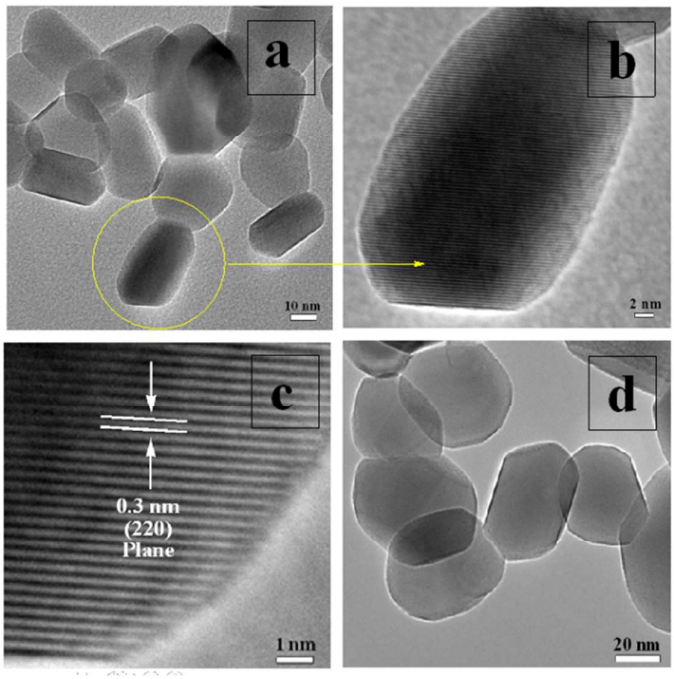

Figure 3. TEM images of a)-c) fresh and d) spent (after 5 recycles) $CuCr_2O_4$ spinel nanoparticles.

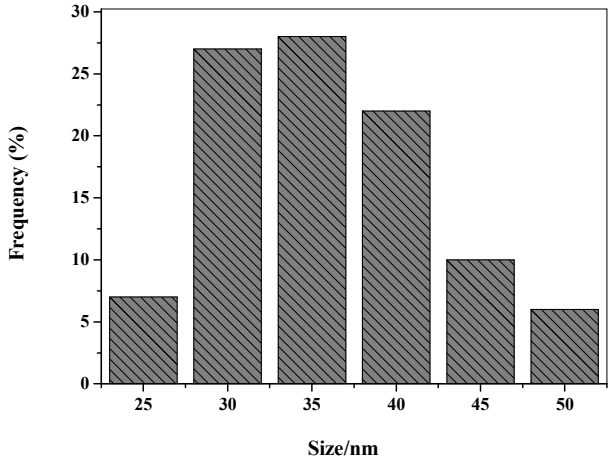

Figure 4. Particle size distribution histogram of the $CuCr_2O_4$ nanoparticles catalyst (from TEM).

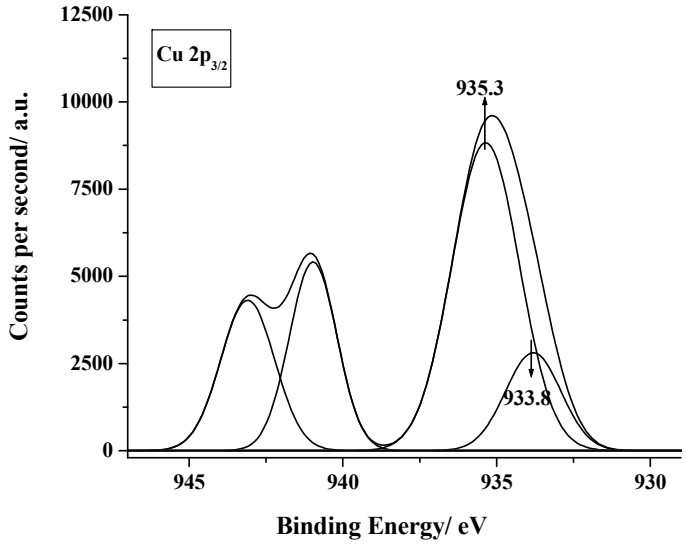

Figure 5. Cu 2p $_{3/2}$ core level spectra of $CuCr_2O_4$ nanoparticles catalyst.

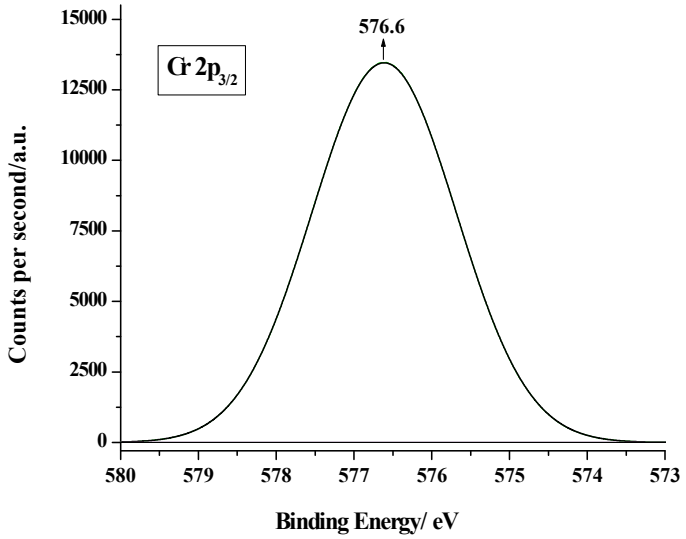

Figure 6. Cr 2p $_{3/2}$ core level spectra of $CuCr_2O_4$ nanoparticles catalyst.

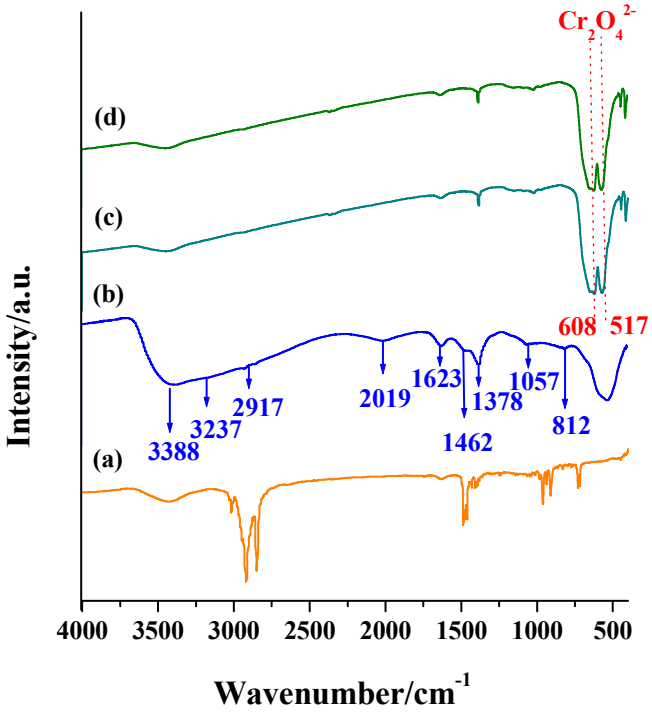

Figure 7. FTIR spectra of (a) pure CTAB (b) uncalcined, (c) calcined and (d) spent (after 5 recycles) $CuCr_2O_4$ spinel catalyst.

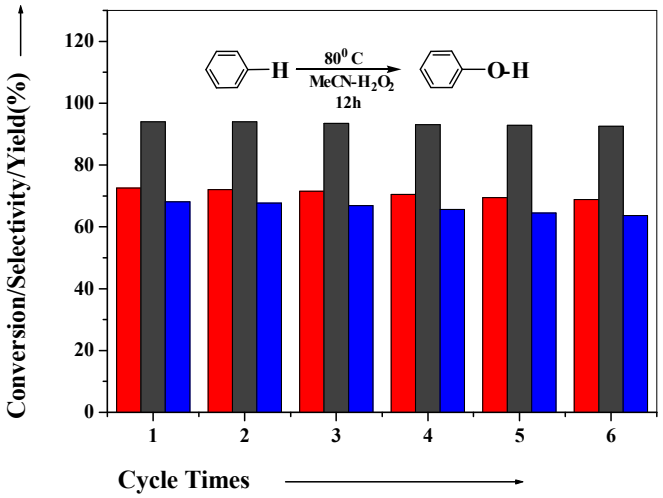

Figure 8. Recyclability tests of $CuCr_2O_4$ spinel nanoparticles catalyst for the hydroxylation of benzene to phenol.

[■] Conversion of benzene; [■] Selectivity to phenol; [■] Yield of phenol.

Reaction Condition: benzene =1g; catalyst= 0.1g; benzene: H_2O_2 mole ratio =1:5; temperature = 80 °C; time =12 h.

Table 1. Physicochemical Properties of the Cu-Cr Catalyst[a]

Entry	Catalyst	Cu/Cr molar ratio	Particle Size (nm)	
			XRD[b] (Crystallite Size)	TEM
1	Fresh catalyst	0.5	38	35
2	Spent catalyst ($CuCr_2O_4$, after 5 recycle)	0.5	37.5	39

[a] Estimated by ICP-AES; [b] Measured using Scherrer equation.

Table 2. Summary of the EXAFS fitting results for Cu-catalysts

Catalyst	Path	Total Path R(10^{-1}nm)	CN	DW (10^{-5}nm^2)
$CuCr_2O_4$ [a]	Cu–O	1.938±0.037	2.5±0.4	2.9±1.1
	Cu–O	1.885±0.025	4	13.1
	Cu–O	3.139	4	17.1
	Cu–Cr	3.243	4	7.3
$CuCr_2O_4$ [b]	Cu–O	1.932±0.058	2.5±0.4	2.2±2.2
	Cu–O	1.881±0.028	4	16.8
	Cu–O	3.133	4	22.0
	Cu–Cr	3.237	4	9.4

[a] Fresh Catalyst: Δk ($10nm^{-1}$) = 3-14, ΔR ($10nm^{-1}$) = 1.0-3.6, ΔE_0 (eV) = -12.4±1, R_f (%) = 2.57;

[b] Spent Catalyst : Δk ($10nm^{-1}$) = 3-13, ΔR ($10nm^{-1}$) = 1.2-3.6, ΔE_0 (eV) = -7.4±2.1, R_f (%) = 1.86.

Table 3. Activities of the Different Catalysts for Benzene Hydroxylation [a]

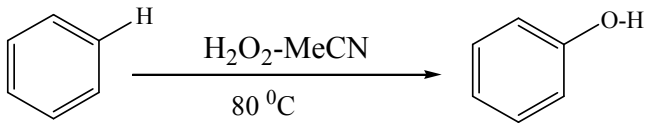

Entry	Catalyst	C_B(%) [b]	S_P(%) [c]			S_H(%) [d]	Y_P(%) [e]	E_o(%) [f]
			Φ_{OH}	Cat	HQ			
1	CuO^{COM}	5.9	5.5	65	29.5	2.8	0.3	0.06
2	Cu_2O^{COM}	6.5	8.0	68	24	4.2	0.5	0.1
3	$Cr_2O_3^{COM}$	7.5	2.0	65	33	1.0	0.1	0.03
4	$CuCr_2O_4^{COM}$	14.5	17.0	48	35	9.3	2.4	0.5
5	$CuO\text{-}Cr_2O_3^{IMP}$	12.3	11.5	55	33.5	6.1	1.4	0.3
6 [g]	$CuO\text{-}Cr_2O_3$	28.2	74.9	15.5	9.6	59.9	21.1	4.2
7 [h]	$CuCr_2O_4^{NP}$	72.5	94	4	2	88.7	68.1	13.6
8 [i]	$CuCr_2O_4^{NP}$	68.8	92.5	5.5	2	86.0	63.7	12.7
9 [j]	$CuCr_2O_4^{NP}$	-	-	-	-	-	-	-
10	No Catalyst	-	-	-	-	-	-	-

[a] Typical reaction conditions: solvent (MeCN) = 10ml, substrate (benzene) = 1g, catalyst= 0.1g, benzene: H_2O_2 (molar ratio) = 1:5, reaction temperature = 80 °C; time = 12 h; [b] C_B = Conversion of benzene based upon the FID-GC using anisole as external standard = [Moles

of benzene reacted/initial moles of benzene used] x 100; [c] S_P = Selectivity to phenol = [Moles of products produced/ moles of benzene reacted] x 100; [d] S_H = Selectivity based on H_2O_2 = [Moles of phenol produced/Moles of converted H_2O_2 × 100] ; [e] Y_P = Yield of phenol= C_B × S_P/100; [f] E_o = H_2O_2 efficiency = [Moles of phenol formed/total moles of H_2O_2 added]× 100; [g] Cu-nanoclusters supported on Cr_2O_3; [h] Prepared $CuCr_2O_4$ spinel nanoparticles and [i] catalyst after 5 reuse; [j] Using 2,6-di-*tert*-butyl-4-methyl phenol as radical scavanger. COM: commercial; IMP: impregnation method; CPM: co-precipitation method; NP: nanoparticles.